INDIAN JOURNAL OF SCIENCE AND TECHNOLOGY

ORIGINAL ARTICLE

Development of CZTS Monograins from Cu_2S, ZnS, and SnS_2 Nanopowders for Solar Cell Application

P Padmapriyanka[1], P Babu[2], K T Ramakrishna Reddy[1]*

1 Solar Photovoltaic Laboratory, Department of Physics, Sri Venkateswara University, Tirupati, 517502, Andhra Pradesh, India
2 Department of Physics, Sri Venkateswara College of Engineering, Karakambadi Road, Tirupati, 517507, Andhra Pradesh, India

OPEN ACCESS

Received: 12/05/2025
Accepted: 30/06/2025
Published: 21/07/2025

Citation: Padmapriyanka P, Babu P, Ramakrishna Reddy KT (2025) Development of CZTS Monograins from Cu_2S, ZnS, and SnS_2 Nanopowders for Solar Cell Application. Indian Journal of Science and Technology 18(28): 2235-2245. https://doi.org/10.17485/IJST/v18i28.885

* **Corresponding author**.

ktrkreddy@gmail.com

Funding: None

Competing Interests: None

Published By Indian Society for Education and Environment (iSee)

ISSN
Print: 0974-6846
Electronic: 0974-5645

Abstract

Objectives: This study describes the preparation of Cu_2ZnSnS_4 (CZTS) monograin layers using binary nanoparticles (NPs) of CuS/ Cu_2S, ZnS, and SnS_2 as precursors. **Methods:** The binary sulfide NPs (CuS/ Cu_2S, ZnS, and SnS_2) were synthesized by relatively inexpensive chemical co-precipitation method using environmentally friendly solvents and chemicals. Two different types of precursor (a) 2CuS + ZnS + SnS_2 and (b) Cu_2S + ZnS + SnS_2 combinations, were used for the preparation of CZTS monograins by tuning all the binaries in a quartz ampoule and heating it. **Findings:** XRD analysis indicated the presence of pure kesterite phase of CZTS, which revealed tetragonal crystal structure for CZTS monograins, when the latter combination was used for sintering at 740 °C for 100 h. This was confirmed by Rietveld refinement analysis and Raman studies. Morphological analysis revealed round shaped grains of approximately 47 μm size that exhibited near stoichiometry. Using CZTS monograins embedded in epoxy resin, solar cell with the device structure Ag/CZTS/CdS/AZO/Ag was fabricated. The evaluated open circuit voltage, short circuit current density, fill factor, and power conversion efficiency of the unoptimized CZTS monograin solar cell were 305 mV, 17.8 mA/ cm^2, 41%, and 2.23%, respectively. These results are presented and discussed. **Novelty**: The CZTS monograins were synthesized by using binary sulfide nanoparticles, which were prepared at low temperatures using simple co- precipitation method for the first time. Further, the analysis of CZTS monograins using Rietveld refinement method to measure the lattice constants, bond angles and bond distances between the atoms of CZTS lattice is new.

Keywords: Binary Sulfide Nanoparticles; Chemical Co- precipitation; XRD; Rietveld refinement; CZTS Monograins; CZTS Solar Cells

1 Introduction

Solar cells present an alternative to the increasing energy needs and environmental challenges. In recent decades, scientists globally have been working to develop high

efficiency thin film solar cells using multinary chalcogenide semiconductors (MCSs). Both the ternary semiconductor I-III-VI_2 combination and the quaternary I_2-II-IV-VI_4 combination offer promising MCSs for technological applications[1]. Significant research has been conducted on copper indium gallium selenide (CIGS) thin-film solar cells, achieving power conversion efficiencies of up to 26.4%[2]. However, indium (In), gallium (Ga), and selenium (Se) have the problem of less abundancy, more toxicity, and high cost, which restricts their use in large-scale production of photovoltaic devices. Copper Zinc Tin Sulfide (Cu_2ZnSnS_4 or CZTS) is a promising alternative quaternary compound for photovoltaic cell development as an absorber layer due to its desirable physical properties and high theoretical solar conversion efficiency (32.2%)[3]. Because of its p-type conductivity, high absorption coefficient (>10^4 cm^{-1}), tuneable energy band gap (1.0 eV-1.6 eV), environmental acceptability, and earth abundancy of the materials involved, kesterite CZTS has recently been recognized as a better replacement for CIGS thin film photovoltaics[4]. The CZTS polycrystalline solar cells exhibited solar power conversion efficiency (PCE) of 8.4%[5], while the CZTS monograin layer (MGL) solar cells achieved a PCE ranging from 9.1% to 12.06%[6]. Additionally, the kesterite CZTSSe thin film solar cells reached a PCE of 14.6%[7]. The physical methods used for synthesis of CZTS monograins from its elemental powders of Cu, Zn, Sn, and S, in the presence of molten flux, are well documented[8]. However, the use of these elemental powders in the synthesis of CZTS monograin leads to several challenges, including (i) the formation of multi-phases, (ii) the requirement for an inert S atmosphere during post-thermal treatment, and (iii) the loss of tin during thermal treatment, necessitating higher processing temperatures. The use of binary precursors in the preparation of CZTS monograins can eliminate these issues. In the fabrication of CZTS thin films four distinct precursor combinations: (i) Cu_2S+ZnS+SnS_2, (ii) Cu_2S+ZnS+SnS, (iii) 2CuS+ZnS+SnS_2, and (iv) 2CuS+ZnS+SnS were used in the literature. These results demonstrated that the production of a single-phase CZTS film with large grains (1μm) occur with the precursor combination of Cu_2S, ZnS, and SnS_2, due to the negative formation energy (-3.67 eV) and favourable oxidation states. In comparison to their bulk counterparts, binary sulfide nanoparticles have better physical characteristics and require low processing temperatures. So that, the high thermal budget can be reduced. Monograin layers (MGLs) provide various benefits compared to traditional thin films, including superior grain boundary passivation, increased light scattering, and improved charge carrier transport, attributable to their uniform grain structure and minimized interfacial defects. Muska et al.[9] synthesized CZTS monograin powder using CuS, SnS and ZnS binary precursors and studied the impact of Co- doping of K and Li on the properties of CZTS monograin powders. Wang et al.[10] synthesized Cd- free pure kesterite CZTS thin film solar cell by magnetron co-sputtering from ZnS, SnS_2 and Cu- targets. However, for the synthesis of binary sulfides (ZnS, SnS/ SnS_2 and CuS/ Cu_2S), they used different techniques that involved expensive equipment, complex procedures, and high temperatures, whereas the co-precipitation technique involved low temperatures, use of minimum chemicals and doesn't require sophisticated equipment. In this context, the current work focuses on the synthesis and characterization of CZTS monograins using such as CuS/ Cu_2S, ZnS and SnS_2 binary sulfide nanoparticles (NPs) by a relatively low-cost chemical co-precipitation method and utilization of these binary precursors in the preparation of CZTS monograin layers for solar cell develpoment. In the preparation of the present work, two different types of precursor combinations such as (a) Cu_2S+ZnS+SnS_2 and (b) 2CuS+ZnS+SnS_2 were used in the synthesis of CZTS monograins. The prepared CZTS monograins were analysed by various characterization techniques. Phase pure CZTS monograins were synthesized from the precursor combination, Cu_2S+ZnS+SnS_2 and employed in the development of CZTS monograin layer solar cells. In the present work, we specially focussed on the Rietveld refinement analysis of the CZTS monograins in greater detail and measured lattice constants, bond angles, bond distances between atoms of CZTS lattice for the first time. This will give a clear picture of the structure of CZTS monograins. Further, the microstructural and morphological details of the monograins were also discussed. Finally, flexible CZTS monograin layer solar cell with Ag/CZTS/CdS/AZO/Ag device structure was developed that showed a maximum power conversion efficiency (PCE) of 2.23% for initial devices.

2 Methodology

Analytical grade CuCl/ $CuSO_4.5H_2O$, $ZnSO_4.7H_2O$, $SnCl_2.2H_2O$, thioacetamide and thiourea, acquired from Sigma- Aldrich were used as precursors for the preparation of CuS / Cu_2S, ZnS and SnS_2 nanopowders using chemical co-precipitation method used in our laboratory as reported earlier[11],[12]. Triethanolamine and Conc. HCl were used as a complexing agent in the synthesis process.

2.1 CZTS monograin synthesis

CZTS monograins were synthesized using CuS/Cu_2S NPs, ZnS NPs, SnS_2 NPs as precursors, and potassium iodide (KI) as a flux material. In a synthesis, for precursor combination of (a) Cu_2S+ZnS+SnS_2, combine 0.7235 g (4.63 mmol) of Cu_2S NPs, 0.4432 g (4.55 mmol) of ZnS NPs, 0.8313 g (4.54 mmol) of SnS_2 NPs, 3.8448 g of KI, and 0.0154 g of elemental sulphur powder (to prevent the sulphur deficiency). These binary NPs were mixed thoroughly, degassed under vacuum, and sealed in quartz

ampoules. The ampoule was heated isothermally at 1013 K for 100 hours in a furnace and then cooled to room temperature. The ampoule was broken, the ingot was powdered, and the flux material was removed by dissolving it in deionised water, and then dried. For the precursor combination of (b) $2CuS+ZnS+SnS_2$, stoichiometric amounts about 0.8700 g (9.01 mmol) of CuS NPs, 0.4432 g of ZnS NPs, and 0.8313 g of SnS_2 NPs were utilized. The next steps are the same as stated above.

Chemical treatments are crucial for enhancing the performance of CZTS monograin solar cells. Various etching agents, such as HCl, KCN, NH_4OH, and Br- methanol, have been employed on Cu_2ZnSnS_4 monograins in the literature to etch the secondary phases[13]. HCl effectively etches Sn, Zn, and S, whereas KCN preferentially etches Cu, Sn, and S. NH_4OH etches copper and sulfur, while Br- methanol etches copper, zinc, and sulfur. HCl etching has been reported to significantly enhance device efficiency compared to devices without etching. This process is useful due to its fewer hazards and more effective than KCN etching. Therefore, the synthesized CZTS monograins were chemically treated using NH_4OH and HCl to remove the binary phases, if any from the crystal surfaces[13] and then washed and dried.

2.2 CZTS monograin layer preparation

The synthesized CZTS monograins were sieved to separate grains of different sizes and then used in the fabrication of CZTS monograin layers. Figure 1 shows the typical synthesis steps involved in the preparation of CZTS monograins and monograins embedded film. To prepare CZTS monograin layers, 0.0457 gm of synthesized CZTS monograins and epoxy resin were mixed well and then mechanically pressed by placing them in between two Teflon plates as depicted in Figure 1. The resulted epoxy layer with CZTS monograins is cleaned with NH_4OH and HCl to remove the stains, dirt and dust before depositing other layers, then washed and dried.

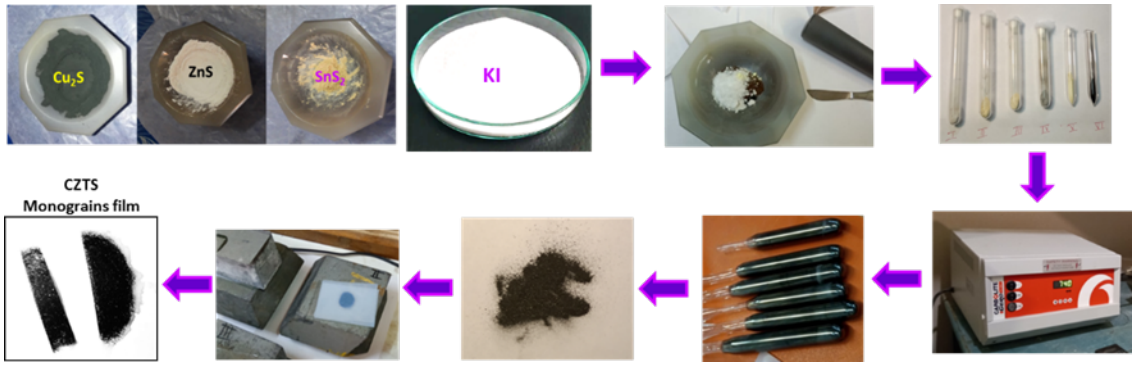

Fig 1. Synthesis steps of CZTS monograins and CZTS monograin films

2.3 Fabrication of CZTS monograin layer solar cells

The synthesized CZTS monograin layers were integrated into solar cells with a device structure of Ag/CZTS/CdS/AZO/Ag. Initially 60 nm thick CdS buffer layer was deposited onto the top of CZTS monograins by using chemical bath deposition (CBD) and dried at 80 °C for two hours in an oven under N_2 ambient. The deposition of CdS layer was carried out using the aqueous solutions of $CdSO_4$ (0.0074 M), 25% ammonia (NH_3 (aq)) and $SC(NH_2)_2$ (0.2M) at a bath temperature of 80°C for a deposition time of 15 min. Next, CZTS monograins coated with CdS layer were embedded into epoxy to form the films. After the formation of CZTS/ CdS monograin layer (MGL), the back side of the MGL was grinded and etched using concentrated sulfuric acid to open up the surfaces of CZTS monograins and then painted by silver (Ag) paste as back contact. On the top of CdS layer, Al-doped ZnO layer of 600 nm thickness was grown using DC-magnetron sputtering. Finally, Ag paste was used as the top ohmic contact.

2.4 Characterization

A Bruker D-5005 diffractometer was used to measure X-ray diffraction of the synthesized samples at 40 kV and 40 mA, using Cu $K_{\alpha 1}$ radiation with $\lambda = 1.5406$Å. Raman spectra were recorded by a Horiba Lab Ram HR 800 high-resolution spectrometer at room temperature using 532 nm laser light in the backscattering configuration. Field-emission scanning electron microscopy (FE-SEM; Ultra 55 FE-SEM Carl Zeiss) was used to examine the morphology of CZTS monograins and composition was measured using energy dispersive spectroscopy (EDS) analysis with an error value of ± 2 at. %, attached to FE-SEM. A Keithley

2400 electrometer under standard test conditions (AM 1.5, 100 mW/ cm^2) was used to evaluate the current versus voltage (I-V) properties of CZTS monograin solar cells.

3 Results and Discussion

3.1 Structural analysis

Figure 2 shows the XRD pattern of CZTS monograins obtained using two different precursor combinations such as (a) 2CuS+ZnS+SnS_2 and (b) Cu_2S+ZnS+SnS_2. From Figure 2(a), it was found that CZTS is formed along with secondary phase of $Cu_{2-x}S$, due to the presence of relatively excess Cu concentration and incomplete conversion of binary sulphides. The Cu_7S_4 ($Cu_{2-x}S$) secondary phase is indeed easily formed in the CZTS. This could generate short circuits and high series resistance, as well as decrease the fill factor of the solar cell device[14]. Figure 2(b) shows the CZTS monograins obtained using Cu_2S+ZnS+SnS_2 precursor combination having a pure kesterite phase of tetragonal unit cell structure with three major peaks positioned at 28.54°, 47.48°, 56.32° that correspond to the (112), (220) and (312) planes respectively and these results agree well with the previous reports[15]. The crystallite size of CZTS was, calculated by Scherrer formula and found as 43.5 nm. The growth of pure CZTS phase without any secondary phases was due to (i) matching of oxidation states in the binary precursors (Cu_2S+ZnS+SnS_2; Cu^{1+}, Zn^{2+}, Sn^{4+}) with that of CZTS (Cu^{1+}, Zn^{2+}, Sn^{4+}), and (ii) complete conversion of binary sulphides owing to low formation energy (-3.67 eV). Therefore, it is much easier to form phase pure CZTS from the precursor combination of Cu_2S+ZnS+SnS_2 compared to 2CuS+ZnS+SnS_2.

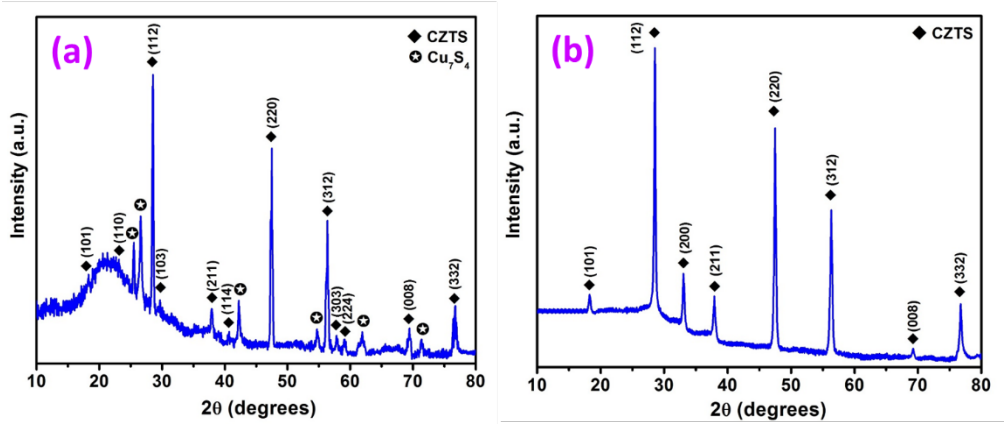

Fig 2. XRD pattern of CZTS monograins obtained using (a) 2CuS+ZnS+SnS_2 and (b) Cu_2S+ZnS+SnS_2

The Rietveld refinement method is utilized for extracting crystal structure information from XRD data. Figuring out structural parameters depend on the total intensity of diffraction peaks. Improving the match between simulated and observed powder diffraction patterns is made easier with the Marquardt least-squares algorithm. Evaluating the enhancement in the minimization process involves analyzing traditional reliability index parameters such as residuals for the weighted pattern (R_{wp}), residuals for the pattern (R_p), Bragg's factor (R_{Bragg}), and Goodness of fit (χ^2). Quantifying the fit between the experimental and calculated diffraction patterns involve numerical values of certain parameters determined by specific mathematical relationships given below.

$$R_{wp} = \left[\frac{\sum_{i=1,n} w_i \left(y_{i(obs)} - y_{i(cal)}\right) 2}{\sum_{i=1,n} w_i \left(y_{i(obs)}\right) 2}\right]^{1/2} \quad (1)$$

$$R_p = \left[\frac{\sum_{i=1,n} |y_{i(obs)} - y_{i(cal)}|}{\sum_{i=1,n} y_{i(obs)}}\right] \quad (2)$$

$$R_{Bragg} = \left[\frac{\sum |I_{(obs)} - I_{(cal)}|}{\sum |I_{(obs)}|}\right] \quad (3)$$

$$R_{exp} = \left[\frac{n-p}{\sum_{i=1,n} w_i \left(y_{i(obs)}\right) 2}\right]^{1/2} \tag{4}$$

$$\chi^2 = \left[\frac{\sum_{i=1,n} w_i \left(y_{i(obs)} - y_{i(cal)}\right) 2}{n-p}\right] = \left[\frac{R_{wp}}{R_{exp}}\right]^2 \tag{5}$$

Based on the equations provided, $y_{i(obs)}$ that stands for the observed intensity while $y_{i(cal)}$ represents the calculated intensity for the i^{th} step, the weight for each experimental observation, w_i, is calculated as the reciprocal of $y_{i(obs)}$. Here, 'n' denotes the overall count of experimental observations, 'p' symbolizes the count of parameters evaluated using the least-square approach, and 'I' stands for the integrated intensity. Figure 3(a & b) shows the Rietveld refinement with acceptable fit quality [χ^2<3] of the XRD patterns of CZTS monograins using the binary nanoparticle combinations of 2CuS+ZnS+SnS_2 and Cu_2S+ZnS+SnS_2 respectively. Lattice parameters, atomic positions, atomic coordinates and residual parameter values were obtained after refinement are listed in Table 1. It was found that Cu_2S+ZnS+SnS_2 combination has a best fit i.e., $\chi^2 = 1.218$, when compared to 2CuS+ZnS+SnS_2 combination, that has a higher χ^2 value of 1.999 which may be due to the presence of secondary phase in the later combination. In this particular instance, the space group was determined to be I-42m, and the peak shape function was decided upon as being pseudo voigt. Gupta et al.[16] and Sultana et al.[17] also measured the Rietveld refinement analysis with lattice parameters, which are close to the present work.

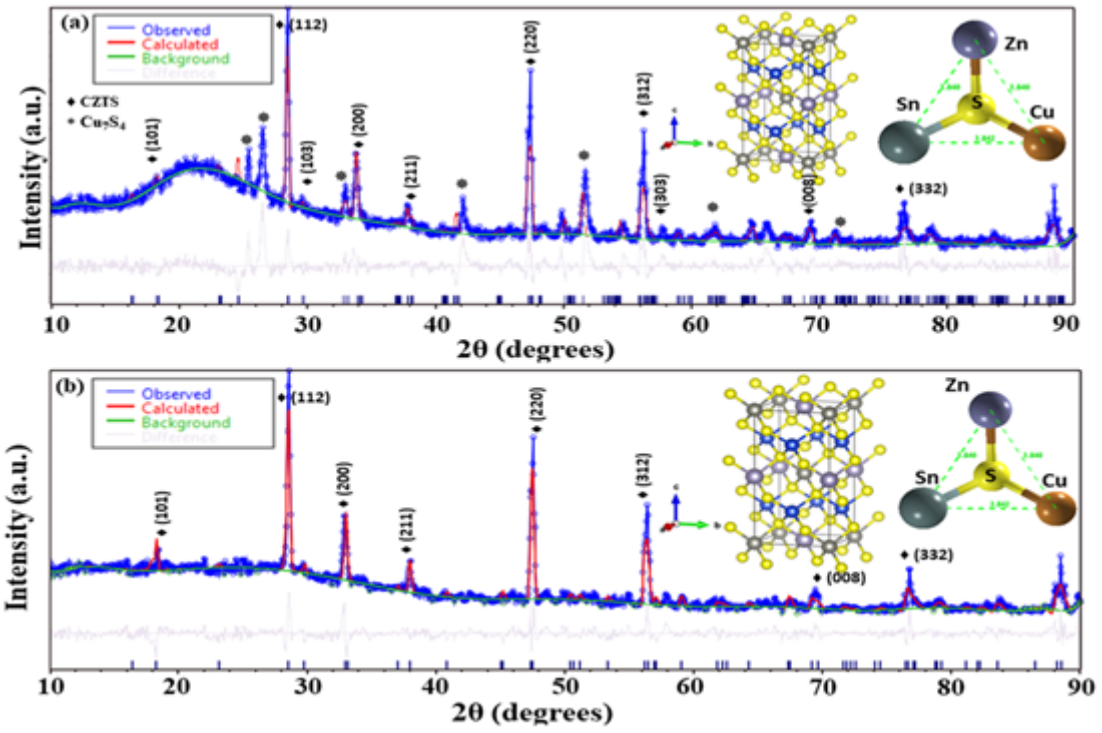

Fig 3. Rietveld refinement analysis of CZTS monograins obtained using different precursor combinations (a) 2CuS+ZnS+SnS_2 and (b) Cu_2S+ZnS+SnS_2

Figure 4 displays the crystalline structure of Cu_2ZnSnS_4 nanoparticles, which have kesterite phase of disordered tetragonal structure with CIF: 9004750 in the I-42m space group. Due to the significant differences in chemical composition and size between copper and tin, there is a noticeable disorder mainly in the copper-zinc sublattice, while the copper-tin layer stays ordered. However, the intricate structure of these quaternary chalcogenides often leads to the presence of different structural defects even at near room temperature. Out of these defects, the most common one is thought to be Cu_{Zn} substitution, as well

Table 1. Structural and lattice parameters of Cu_2ZnSnS_4 nanoparticles calculated using Rietveld refinement

Sample	a = b (Å)	c (Å)	χ^2	R_p	Cell volume (Å)^3		c/ 2a
					Calculated	Theoretical	
2CuS + ZnS + SnS_2	5.396	10.791	1.999	14.730	317.77	319.50	1.000
Cu_2S + ZnS + SnS_2	5.433	10.830	1.218	9.348	318.01	319.50	1.000

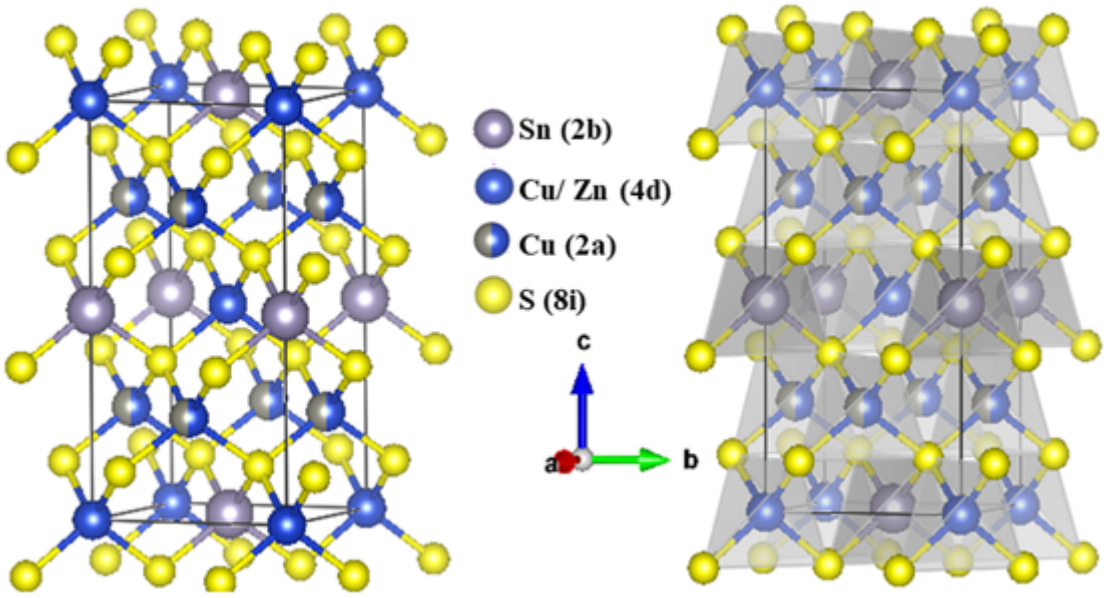

Fig 4. Crystalline structure of normal and polyhedron view of Cu_2ZnSnS_4 nanoparticles

as copper vacancies, which lead to the p- type characteristic of kesterite structure with the lowest formation energy compared to other defects[18].

Table 2 shows the main interatomic bond distances between Cu/Zn(4d)- Cu(2a) was 3.826 Å, and between Cu(2a)-Sn(2b) was 3.838 Å, whereas the interatomic distances for Cu/Zn(4d)-S(8i), Cu(2a)-S(8i), Sn(2b)-S(8i) and Cu/Zn(4d)-Sn(2b) were 2.335 Å, 2.332 Å, 2.409 Å and 3.840 Å respectively. It was clear that there is no direct bond between homo (Cu- Cu; Cu/ Zn- Cu/ Zn and Sn - Sn) and hetero (Cu- Cu/Zn; Cu- Sn; Cu/ Zn- Sn) molecules and these are interconnected with surrounding sulphur atom at various bond angles and interfacial bond angles, atomic positions of various atoms, which are listed in Table 3. The structures of both 2CuS+ZnS+SnS_2 and Cu_2S+ZnS+SnS_2 nanoparticles have different stoichiometries and compositions based on the close thermodynamic stability of the oxidation states of Cu (2a), Cu/ Zn (4d) and Sn (2b) and are tetrahedrally coordinated through sulphur lattice in symmetry with an I-42m (121) space group.

From Table 3, the parameters of the tetrahedraon Cu/Zn(4d), Cu(2a) and Sn(2b) are observed with data from the refinement analysis of Cu_2ZnSnS_4 monograins. It was possible to identify the significant difference between the angles of inclination of tetrahedron, average bond length, polyhedron volume and x, y and z positions of sulphur.

3.2 Raman analysis

Raman analysis can be used for identification of additional phases and confirm the phase purity of synthesized CZTS monograins. Figure 6(a) and **6**(b) showed the Raman spectra of CZTS monograins using 2CuS+ZnS+SnS_2 and Cu_2S+ZnS+SnS_2 precursor combination. From Figure 6(a), a strong peak observed at 339 cm^{-1} which was attributed to the A1 symmetry mode of kesterite CZTS and is related with vibration of 'S' atoms[16]. The peaks present at 257 cm^{-1} and 474 cm^{-1}, correspond to $Cu_{2-x}S$, which confirm the existence of a secondary phase[2] due to the mismatching of oxidation states in binary precursors with that of CZTS.

However, Figure 6(b) shows that all the peaks are related to pure kesterite phase of CZTS, without any secondary phases. The peaks observed at 255, 287, 338 and 367 cm^{-1} are in good agreement with the earlier reports[17]. The major peak at 338 cm^{-1} is attributed with A1 vibrational mode which occurs in the sulphur atoms of CZTS lattice[16]. Balakrishna et al.[19] also showed the

Table 2. Interatomic distances of tetrahedra and its calculated inter- atomic bond angles and atomic positions

Interatomic distances of bonds in tetrahedra

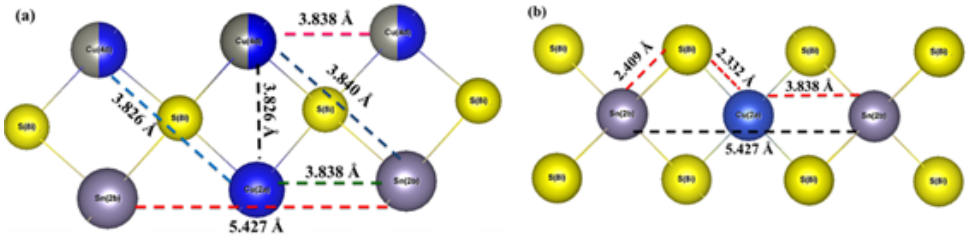

Inter-atomic Bond Angles

Type	Start Atom	Vertex	End Atom	Angle	
Cu – S – Cu	Cu/ Zn (4d)		S (8i)	Cu (2a)	110.75
Cu – S – Sn	Cu/ Zn (4d)		S (8i)	Sn (2b)	108.10
Cu – S – Sn	Cu (2a)		S (8i)	Sn (2b)	108.26
Cu – Sn – S	Cu/ Zn (4d)		Sn (2b)	S (8i)	35.297
Cu – Cu – S	Cu/ Zn (4d)		Cu (2a)	S (8i)	34.642

Atomic Positions of Cu_2ZnSnS_4

Lable	Type	X	Y	Z	B
Cu (4d)	Cu	0.500	1.00	0.750	1.02644
Zn(4d)	Zn	0.500	1.00	0.750	1.02644
Cu (2a)	Cu	1.00	1.00	1.00	1.19699
Sn (2b)	Sn	0.500	0.500	1.00	0.56138
S (8i)	S	0.75617	0.75617	0.872	0.61192

Table 3. Structural parameters of the tetrahedron with Cu (2a), Cu/ Zn (4d), Sn (2b) atoms at the centre of the unit cell and its distance (Å) to S (8i)

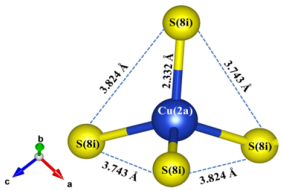

Avg. Bond Length = 2.325 Å
Polyhedral Volume = 6.444 Å^3

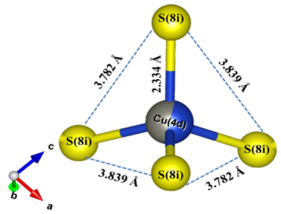

Avg. Bond Length = 2.328 Å
Polyhedral Volume = 6.469 Å^3

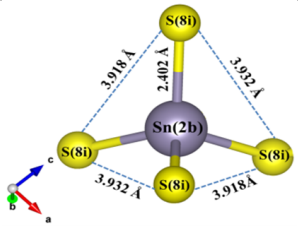

Avg. Bond Length = 2.402 Å
Polyhedral Volume = 7.113 Å^3

	x	y	z		x	y	z		x	y	z
S(8i)	- 0.244	0.756	1.128	**S(8i)**	0.244	0.244	0.128	**S(8i)**	- 0.256	- 0.256	0.628
S(8i)	- 0.244	1.244	0.721	**S(8i)**	0.256	- 0.256	0.372	**S(8i)**	- 0.256	0.256	0.372
S(8i)	0.244	0.756	0.872	**S(8i)**	0.744	0.256	0.372	**S(8i)**	0.256	- 0.256	0.372
S(8i)	0.244	1.244	1.128	**S(8i)**	0.756	- 0.244	0.128	**S(8i)**	0.256	0.256	0.628

strongest peak of CZTS nanoparticles at 338 cm^{-1} due to scattering from kesterite CZTS, which shows similar peak to support our Raman results. In addition, the peak at 367 cm-1 was related to the symmetrical movement of the sulphur anion grid with respect to the Sn, Zn and Cu atoms [20]. Peaks corresponding to binary and ternary components like ZnS, $Cu_{2-x}S$, Cu_2SnS_3 phases having peaks at 278 cm^{-1}, 257 cm^{-1}, 474 cm^{-1}, 351 cm^{-1}, 303 cm^{-1} and 355 cm^{-1} are not observed in the Cu_2S+ZnS+SnS_2 precursor combination, confirming that the synthesized monograins had the pure kesterite phase of CZTS. Hence the Raman analysis results supported the XRD data.

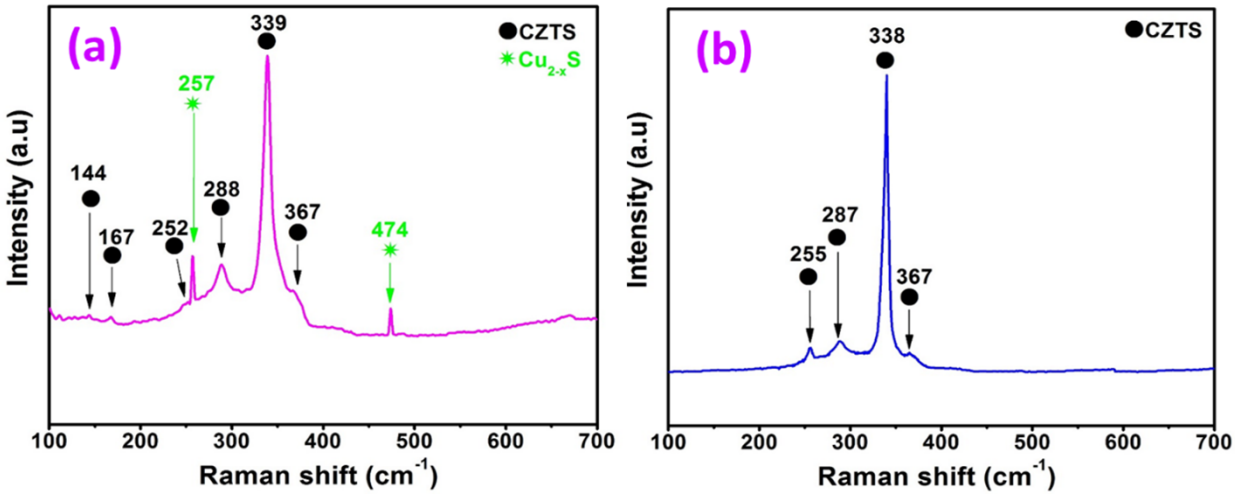

Fig 5. Raman Spectra of CZTS monograins synthesized using different precursor combinations (a) 2CuS+ZnS+SnS_2 and (b) Cu_2S+ZnS+SnS_2

3.3 Morphological and Composition analysis

The SEM image (Figure 6(a)) of CZTS monograins obtained from the precursor combination of 2CuS+ZnS+SnS_2 showed non-uniform and aggregated growth of the monograins. This growth indicates the incomplete conversion of binary sulphides due to the relatively high formation energy (-1.68 eV). However, a round shaped, uniform and compact grains of 47 μm size with less faceting were obtained as seen in Cu_2S+ZnS+SnS_2 precursor combination (Figure 6 (b&c)). Few grains were subjected to secondary agglomeration due to either longer growth time or higher heating temperature used during the synthesis process. To restrict the secondary agglomeration, growth time must be optimized, and those studies are in progress. It is necessary to synthesize uniform, round-shaped, and smooth-surfaced CZTS monograins for the application of high-efficiency solar cells. Therefore, it was clearly indicated that the CZTS monograins from Cu_2S+ZnS+SnS_2 precursor combination was better utilized in the development of CZTS-based monograin solar cells.

Figure 6(d) illustrates the EDS colour mapping elemental analysis of CZTS monograins, which indicates the homogeneous distribution of Cu (Red), Zn (Gold), Sn (Thick green) and S (Green) as the only elements over a wide area range (20μm) with atomic (%), showed that [Zn]/[Sn] = 1.04 and [Cu]/([Zn] + [Sn]) = 0.98 for 2CuS+ZnS+SnS_2 precursor combination, which indicates a slightly higher Cu-content in the sample. The obtained copper-rich composition led to the presence of Cu_7S_4 ($Cu_{2-x}S$) secondary phase, which is also evident from the XRD and Raman analysis. Similarly, the initial composition of precursors can also be showed a major impact on the monograins formation. The EDS analysis of Cu_2S+ZnS+SnS_2 binary sulfides combination showed [Zn]/[Sn] = 1.01 and [Cu]/([Zn] + [Sn]) = 0.92, which are close to the desired stoichiometric values of Cu, Zn, Sn, and S in CZTS. Nagamalleswari et al. [21] reported that the ratio of [Cu]/([Zn] + [Sn]) varied from 1.13 to 0.92 for slightly Cu-deficient, which indicated that the CZTS solar cells with high conversion efficiencies are possible with monograins. Here Cu-poor CZTS reduce the secondary phases and Cu-poor, Zn-rich condition is desirable for better performance of CZTS solar cell [22].

3.4 CZTS monograin solar cells

The CZTS monograins synthesized by using Cu_2S+ZnS+SnS_2 precursor combination was integrated into solar cells with a device configuration of Ag/CZTS/CdS/AZO/Ag. Figure 7 displays the illuminated current versus voltage (I-V) characteristics

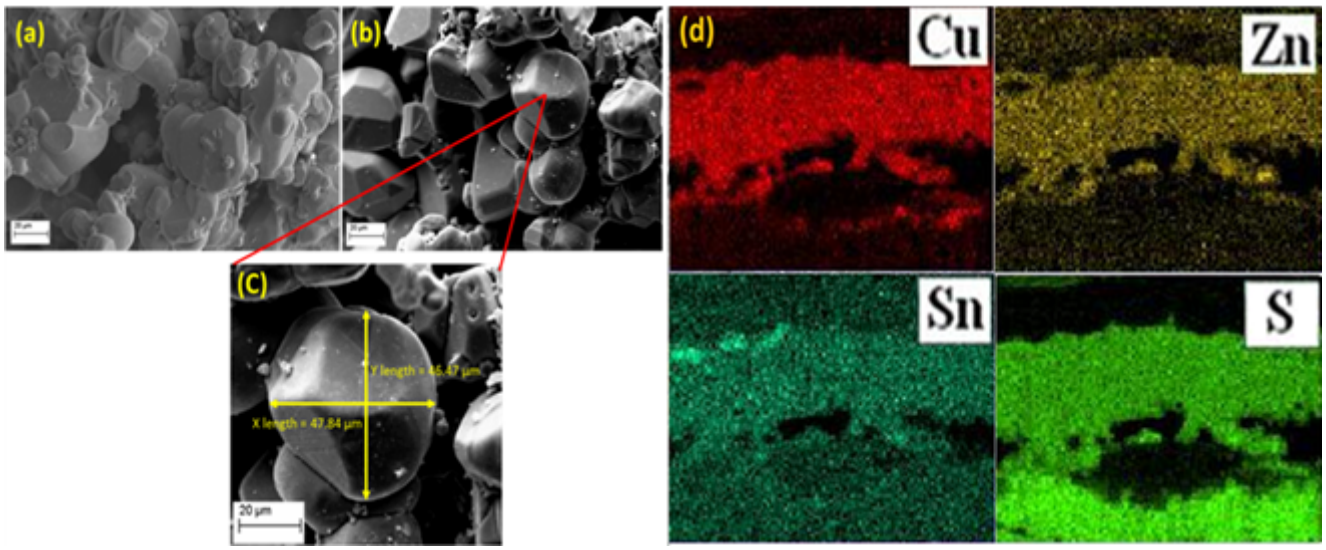

Fig 6. SEM images synthesized using different precursor combinations (a) 2CuS+ZnS+SnS_2 ,(b) Cu_2S+ZnS+SnS_2, (c) enlarged view of CZTS monograin from Figure (b) and (d) Elemental colour mapping images of CZTS monograins

of CZTS monograin solar cell using a lamp source of 100 mW/Cm^2 intensity and the inset of the figure shows the cross-section of the fabricated solar cell. The fabricated CZTS monograin solar cells showed an open-circuit voltage, V_{oc} = 305 mV, short-circuit current density, J_{sc} = 17.8 mA/cm^2, fill factor, FF = 41%, and solar power conversion efficiency, η of 2.23% for the total area of 1 cm^2. As the CZTS monograins were embedded in epoxy, it is difficult to estimate the active area in the monograin solar cells.

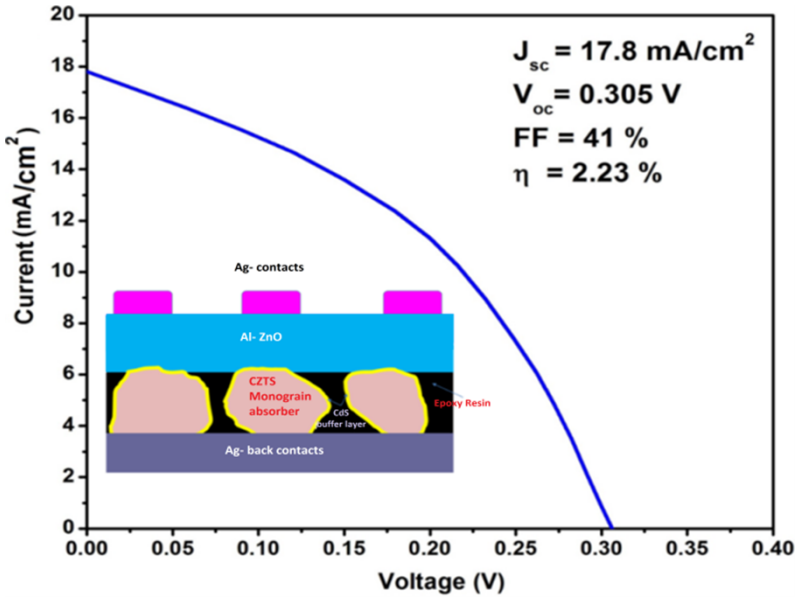

Fig 7. Light-illuminated I-V characteristic of CZTS monograin solar cell

The comparatively high J_{sc} value observed in this study suggests the high quality of CZTS monograins as a light absorber. However, the resulting low efficiency of the fabricated CZTS monograin solar cell was primarily due to lower fill factor and V_{oc}. These deficiencies are often linked to high series resistance and low shunt resistance, presence of defects, interface recombinations, atomic disorder and inadequate electrical properties of window layers[23]. Generally, low FF is aided by high series resistance whereas the low band gap leads to a decrease in V_{oc}[7]. Usually, Zn-rich and Cu-poor compositions are

desirable to develop highly efficient CZTS solar cells[22]. To improve the power conversion efficiency, various reasons such as metal contact layer materials effect, defect formation of Cu and Zn with negative energy formation, crystal disorder, low diffusion length of electrons in p-type material, recombination mechanism in the interface and optical losses etc.,[24] which will improve the FF and V_{oc}. Those studies are in progress. Rajeshmon et al.[25] synthesized CZTS/In_2S_3 junction thin film solar cell using spray pyrolysis by varying Cu and Sn concentration and obtained a conversion efficiency of 1.85%. Solar cells with 8.4% and 9.4% efficiency were achieved by synthesizing CZTS monograin layers. Here the monograins were prepared using KI flux and upon Li and K co-doping, as reported by Muska et al.[10]. Fathima et al.[24] prepared solar cells using the structure, FTO/Ag/CdS/CZTS/Ag with ZnS as an antireflection coating through spray pyrolysis and observed that the sulfurization temperature optimization can increase the efficiency from 0.21% to 0.45%. However, the present study indicates that use of binary sulfide nanoparticles (NPs) for the preparation of CZTS monograins is beneficial and has the potential to pave the way for mass-production of CZTS monograin solar cells. The usage of binary NPs can be synthesized at lower processing temperatures than the traditional method, which reduce the cost of synthesizing CZTS monograins. In addition, the use of binary NPs could also improve the quality of CZTS monograins and led to fewer defects compared to the thin films, which could improve the efficiency and performance of the solar cells. Hence CZTS monograin solar cells prepared using simple and economic methods could be more useful in the development of cost effective monograin solar cells although these cells are less efficient compared to more efficient cell technology that is costlier.

4 Conclusion

CZTS monograin layers were synthesized using binary precursors of CuS/Cu_2S, ZnS and SnS_2 nanoparticles. These binary precursors were grown by a relatively in-expensive chemical co-precipitation technique using eco-friendly solvents and chemicals. Two different precursor combinations such as (a) 2CuS+ZnS+SnS_2 and (b) Cu_2S+ZnS+SnS_2 are used for the preparation of CZTS monograins. The XRD and Rietveld refinement analysis results showed that both precursor combinations exhibited kesterite phase of tetragonal crystal structure with a crystallite size of 43.5 μm. The Raman spectra confirmed that Cu_2S+ZnS+SnS_2 precursor combination had the pure kesterite phase of CZTS without any secondary phases. The SEM studies revealed that round-shaped compact grains with less faceting having grain size of 47μm. Finally, the CZTS monograin layered solar cell was fabricated with the device configuration Ag/CZTS/CdS/AZO/Ag that showed a power conversion efficiency of 2.23%. In the present study, binary sulfide nanoparticles were used as precursors to synthesize CZTS monograins, which provide large interface area and led to faster diffusion of atoms or ions. Therefore, in order to restrict the secondary agglomeration, growth time must be optimized, and it is in the progress. The low efficiency of the fabricated unoptimized CZTS monograin solar cell was due to low FF and V_{oc}, which might be due to bulk and interface recombination. Further optimization of CZTS monograin layer, an in-depth investigation of the junction behaviour, type of interface layers and their relative thickness as are needed in order to achieve highly efficient CZTS monograin solar cells.

5 Acknowledgement

The authors would like to thank the ”DEPARTMENT OF SCIENCE & TECHNOLOGY, Ministry of Science & Technology, Government of India” (No. DST/INT/RMES/P-11/2016) in collaboration with the ”RUSSIAN MINISTRY OF EDUCATION AND SCIENCES (RMES)” Government of Russia for financial assistance.

5.1 Authorship contribution

P. Padmapriyanka: Conceptualization, Methodology, Writing- original draft preparation, Formal analysis, Writing – review & editing. P. Babu: Data curation, Software, Writing – review & editing. K.T. Ramakrishna Reddy: Supervision, Visualization, Writing – review & editing.

5.2 Conflict of Interests

The authors do not have any conflicts of interest.

References

1) Suryavanshi PS, Panchal CJ. Low-cost fabrication of single chalcogenide CuInGaSe2 sputter target and its thin films for solar cell applications. *Journal of Optics*. 2024;53:828–846. https://doi.org/10.1007/s12596-023-01324-5.
2) Nagamalleswari D, Kumar YBK, Ganesh V. Effect of substrate temperature on the growth of CuSbS2 thin films by chemical spray pyrolysis. *Physica B: Condensed Matter*. 2021;616:413119. https://doi.org/10.1016/j.physb.2021.413119.

3) Lie S, Leow SW, Bishop DM, Guc M, Izquierdo-Roca V, Gunawan O, et al. Improving Carrier-Transport Properties of CZTS by Mg Incorporation with Spray Pyrolysis. *ACS Applied Materials & Interfaces*. 2019;11:25824–25832. https://doi.org/10.1021/acsami.9b05244.
4) Kois J, Polivtseva S, Mamedov D, Samieipour A, Zh S. Visible light-assisted instability of kesterite Cu2ZnSnS4: What are the implications? *Solar Energy Materials and Solar Cells*. 2020;208:110384. https://doi.org/10.1016/j.solmat.2019.110384.
5) Pal K, Singh P, Bhaduri A, Thapa KB. Current challenges and future prospects for a highly efficient (>20%) kesterite CZTS solar cell: A review. *Solar Energy Materials and Solar Cells*. 2019;196:138–156. https://doi.org/10.1016/j.solmat.2019.03.001.
6) Kauk-Kuusik M, Timmo K, Pilvet M, Muska K, Danilson M, Krustok J, et al. Cu2ZnSnS4 monograin layer solar cells for flexible photovoltaic applications. *Journal of Material Chemistry A*. 2023;11:23640–23652. https://doi.org/10.1039/D3TA04541B.
7) Li Y, Cui C, Wei H, Shao Z, Wu Z, Zhang S, et al. Suppressing Element Inhomogeneity Enables 14.9% Efficiency CZTSSe Solar Cells. *Advanced Materials*. 2024;36:2400138. https://doi.org/10.1002/adma.202400138.
8) Bette S, Isotta E, Mukherjee B, Schulz A, Dallos Z, Kolb U, et al. Microstructural Insights into the Transformation of Cubic, Low-Temperature, Disordered Cu2ZnSnS4 into the Tetragonal Form. *The Journal of Physical Chemistry C*. 2024;128(4):1717–1727. https://doi.org/10.1021/acs.jpcc.3c07085.
9) Muska K, Timmo K, Pilvet M, Kaupmees R, Raadik T, Mikli V, et al. Impact of Li and K co-doping on the optoelectronic properties of CZTS monograin powder. *Solar Energy Materials and Solar Cells*. 2023;252:112182. https://doi.org/10.1016/j.solmat.2023.112182.
10) Wang A, Huang J, Cong J, Yuan X, He M, Li J, et al. Cd-Free Pure Sulfide Kesterite Cu2ZnSnS4 Solar Cell with Over 800 mV Open-Circuit Voltage Enabled by Phase Evolution Intervention. *Advanced Materials*. 2024;36:2307733. https://doi.org/10.1002/adma.202307733.
11) Pegallapati P, Reddivari M, Pejjai B, Kummara T, Kotte TRR. Synthesis of Cu-doped ZnS nano-powder by chemical co-precipitation process. *Materials Today: Proceedings*. 2023. https://doi.org/10.1016/j.matpr.2023.02.419.
12) Pejjai B, Reddivari M, Kotte TRR. Phase controllable synthesis of CuS nanoparticles by chemical co-precipitation method: Effect of copper precursors on the properties of CuS. *Materials Chemistry and Physics*. 2020;239:122030. https://doi.org/10.1016/j.matchemphys.2019.122030.
13) Timmo K, Altosaar M, Pilvet M, Mikli V, Grossberg M, Danilson M, et al. The effect of Ag alloying of Cu2(Zn,Cd)SnS4 on the monograin powder properties and solar cell performance. *Journal of Materials Chemistry A*. 2019;7:24281–24291. https://doi.org/10.1039/c9ta07768e.
14) Amrillah T, Ghariy G. Cu2ZnSnS4 microflower doped Cr and its potential application for solar cell devices. *Journal of Alloys and Compounds*. 2025;1016:178915. https://doi.org/10.1016/j.jallcom.2025.178915.
15) Mahewar RB, Ravangave LS. Structure, morphology and optical parameters of spray deposited CZTS thin films for solar cell applications. *Indian Journal of Science and Technology*. 2020;13(21):2149–2156. https://doi.org/10.17485/IJST/v13i21.642.
16) Gupta AKS, Farhad SFU, Habib MS, Hossan MR, Hossain K, Das NK, et al. Characterizations of extrinsically doped CZTS thin films for solar cell absorbers fabricated by sol-gel spin coating method. *Applied Surface Science Advances*. 2023;13:100352. https://doi.org/10.1016/j.apsadv.2022.100352.
17) Sultana M, Sharmin A, Alam MR, Ahmed S, Shaikh MAA, Bashar MS. Formulation and validation of mathematical model for co-sputtering conditions to attain stoichiometric CZTS films: Expedience of using all metal sulfide targets. *Heliyon*. 2025;11(2):e41758. https://doi.org/10.1016/j.heliyon.2025.e41758.
18) Isotta E, Syafiq U, Ataollahi N, Chiappini A, Malerba C, Luong S, et al. Thermoelectric Properties of CZTS Thin Films: Effect of Cu-Zn Disorder. *Physical Chemistry Chemical Physics*. 2021;23:13148–13158. https://doi.org/10.1039/D1CP01327K.
19) Ananthoju B, Mohapatra J, Bahadur D, Medhekar NV, Aslam M. Influence of the Cu2ZnSnS4 nanoparticles size on solar cell performance. *Solar Energy Materials and Solar Cells*. 2019;189:125–132. https://doi.org/10.1016/j.solmat.2018.09.028.
20) Kandare SP, Dahiwale SS, Dhole SD, Rao MN, Rao R. Order-disorder transition in Nano-Cu2ZnSnS4: a Raman spectroscopic study. *Materials Science in Semiconductor Processing*. 2019;102:104594. https://doi.org/10.1016/j.mssp.2019.104594.
21) Nagamalleswari D, Kumar YBK, Kiran YB, Babu GS. Preparation and Characterization of Cu2ZnSnS4 Thin Films by Two-Stage Process. *Energy Sources, Part A: Recovery, Utilization, and Environmental Effects*. 2019;41(24):3001–3012. https://doi.org/10.1080/15567036.2019.1583294.
22) Nagamalleswari D, Kumar YBK. Growth of Cu2ZnSnS4 Thin Film Solar Cells Using Chemical Synthesis. *Indian Journal of Science and Technology*. 2022;15(28):1399–1405. https://doi.org/10.17485/IJST/v15i28.194.
23) Gupta I, Singla S, Kanjariya P, Jain R, Mohanty BC, Nayak M. Influence of Sulfurization Temperature on Grain Growth in Cu2ZnSnS4 Thin Films Synthesized for Solar Cell Applications. *Physica Scripta*. 2024;99(10):105979. https://doi.org/10.1088/1402-4896/ad764c.
24) Fathima MI, Arulanantham AMS, Wilson KSJ. Effect of ZnS Nanowire ARC on CZTS/CdS Thin Film Solar Cell by Nebulizer Spray Pyrolysis Technique. *Materials Research Express*. 2020;7(1):015510. https://doi.org/10.1088/2053-1591/ab63f9.
25) Rajeshmon VG, Vijayakumar KP, Kartha CS. Effect of Cu and Sn Concentration on the Performance of All-Sprayed CZTS Solar Cell. *Journal of Physics: Conference Series*. 2020;1461(1):012181. https://doi.org/10.1088/1742-6596/1461/1/012181.